PTEP

Prog. Theor. Exp. Phys. **2022** 113B06(13 pages)
DOI: 10.1093/ptep/ptac144

IYBSSD2022
International Year
of Basic Sciences
for Sustainable Development

Muon ($g-2$) and the W-boson mass anomaly in a model based on Z_4 symmetry with a vector-like fermion

Simran Arora, Monal Kashav, Surender Verma*, and B. C. Chauhan

Department of Physics and Astronomical Science, Central University of Himachal Pradesh, Dharamshala 176215, India

*E-mail: s_7verma@yahoo.co.in

Received August 16, 2022; Revised October 14, 2022; Accepted November 2, 2022; Published November 4, 2022

The latest results of the CDF-II Collaboration show a discrepancy of 7σ with standard model expectations. There is also a 4.2σ discrepancy in the measurement of the muon magnetic moment reported by Fermilab. We study the connection between neutrino masses, dark matter, the Muon ($g-2$) experiment, and the W-boson mass anomaly within a single coherent framework based on a Z_4 extension of the scotogenic model with a vector-like lepton (VLL). Neutrino masses are generated at the one-loop level. The inert doublet also provides a solution to the W-boson mass anomaly through correction in oblique parameters S, T, and U. The coupling of the VLL triplet ψ_T to the inert doublet η provides a positive contribution to the muon anomalous magnetic moment. In the model, the VLL triplet provides a lepton portal to dark matter, η_R^0. The model predicts a lower bound m_{ee} > 0.025 eV at 3σ, which is well within the sensitivity reach of the $0\nu\beta\beta$ decay experiments. The model explains the muon anomalous magnetic moment Δa_μ for $1.3 < y_\psi < 2.8$ and a DM candidate mass in the range 152 GeV $< M_{\eta_R^0} <$ 195 GeV. The explanation of the W-boson mass anomaly further constrains the mass of the DM candidate, $M_{\eta_R^0}$, in the range 154 GeV $< M_{\eta_R^0} <$ 174 GeV.

Subject Index B40

1. Introduction

The existence of dark matter (DM), non-zero neutrino masses, and matter–antimatter asymmetry suggests that the standard model (SM) of particle physics, despite its enormous triumphs, cannot be regarded as a conclusive hypothesis. Very recently, the Muon ($g-2$) Collaboration at Fermilab has reported the measurement of the muon anomalous magnetic moment $a_\mu \equiv (g_\mu - 2)/2$, showing a 4.2σ discrepancy with the SM prediction [1]. The difference between the combined experimental result $a_\mu^{\rm exp} = 116\,592\,061(41) \times 10^{-11}$ [1] and the SM prediction $a_\mu^{\rm SM} = 116\,591\,810(43) \times 10^{-11}$ [2] of the muon anomalous magnetic moment is $\Delta a_\mu \equiv a_\mu^{\rm exp} - a_\mu^{\rm SM} = 251(59) \times 10^{-11}$, which is a sign of new physics (NP) beyond the SM (BSM). Several models have been proposed with an aim to accommodate the Muon ($g-2$) result. Although there exist theoretical models based on discrete symmetries to resolve the muon

Funded by SCOAP[3]. SCOAP3 and OUP support the goals of the International Year of Basic Sciences for Sustainable Development

Table 1. The field content and respective charge assignments of the model under $SU(2)_L \times U(1)_Y \times Z_4 \times Z_2$.

Symmetry group	L_e, L_μ, L_τ	e_R, μ_R, τ_R	N_1, N_2, N_3	ψ_T	H	S	η
$SU(2)_L \times U(1)_Y$	(2, −1/2)	(1, −1)	(1, 0)	(3, −1)	(2, 1/2)	(1, 0)	(2, 1/2)
Z_4	$(1, i, -i)$	$(1, i, -i)$	$(1, i, -i)$	i	1	$-i$	1
Z_2	+	+	−	−	+	+	−

anomaly [3–6], the most general framework includes the extension of the SM by $U(1)_{L_\mu - L_\tau}$ symmetry [7,8], wherein an additional gauge boson provides a correction to the muon magnetic moment at the one-loop level [9–15].

Within the SM, the mass of the W-boson is $M_{\mathrm{W}}^{\mathrm{SM}} = 80.354 \pm 0.007$ GeV [16]; however, the CDF-II Collaboration has recently published their results for the mass of the W gauge boson $M_{\mathrm{W}} = 80.4335 \pm 0.0094$ GeV [17], which shows a 7σ discrepancy with the corresponding SM prediction [16]. There have been many attempts to resolve this anomaly [18–28]. The authors of Refs. [29–43] have attempted to provide a common explanation for both the Muon $(g-2)$ result and the W-boson mass anomaly.

In the context of scotogenic models, $U(1)_{L_\mu - L_\tau}$ symmetry has been employed, where a new gauge boson emanating from the symmetry breaking explains the Muon $(g-2)$ result [44–48]. In such scenarios, the scotogenic fields (η, N_k) do not contribute to Muon $(g-2)$ explicitly. Alternatively, in the present work, Z_4 symmetry is employed for the coupling of the muon to the inert doublet η and the vector-like lepton (VLL), ψ_T, explaining the Muon $(g-2)$ result in the framework of the scotogenic model [49–51]. The novelty of the framework lies in the fact that the inert doublet (η) contributes to the neutrino mass, dark matter, Muon $(g-2)$, and the W-boson anomaly explanation. With the addition of three right-handed neutrinos and an inert doublet, the scotogenic model offers a simultaneous explanation for dark matter and non-zero neutrino masses. A scalar singlet is added to the particle content of the model that breaks the Z_4 symmetry. The inert doublet and right-handed neutrinos are odd under the Z_2 symmetry stabilizing the lightest DM candidate, i.e., the real part of the inert doublet in the model. The neutrino masses are generated at the one-loop level. In order to accommodate Muon $(g-2)$, a VLL triplet is added, which couples to the scalar doublet, resulting in a chirally enhanced positive contribution to Muon $(g-2)$ and also providing a lepton portal to DM. In addition, the model can resolve the W-boson mass anomaly through correction in oblique parameters S, T, and U, reflecting the NP contribution.

The paper is organized as follows. In Sect. 2, we discuss the basic structure and phenomenological consequences of the scotogenic model. In Sect. 3, we outline the numerical analysis and related discussion. Finally, in Sect. 4, we summarize our results.

2. Scotogenic model for neutrino masses

We have extended the SM gauge symmetry by a Z_4 symmetry. In order to generate small neutrino masses, we have considered a scotogenic model that extends the SM with three right-handed neutrinos and an inert scalar doublet with an imposed Z_2 symmetry that also provides a solution to DM. The particle content of the model with corresponding charge assignments is given in Table 1. Here, L_α and $\alpha_R (\alpha = e, \mu, \tau)$ are left-handed lepton doublets and right-handed

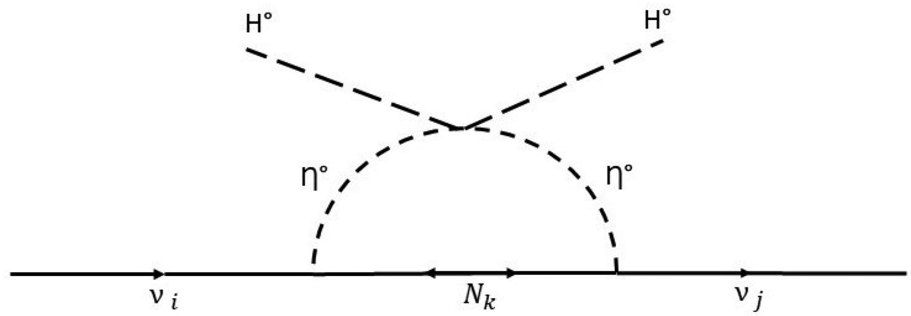

Fig. 1. A diagram showing the neutrino mass generation in the scotogenic model at the one-loop level.

charged leptons, respectively, N_k ($k = 1, 2, 3$) are right-handed neutrino singlets, ψ_T is the VLL triplet, H is the SM Higgs, S is a scalar singlet, and η is an inert scalar doublet.

The relevant terms in the Yukawa Lagrangian are

$$-\mathcal{L} \supseteq \frac{M_{11}}{2} N_1 N_1 + M_{23} N_2 N_3 + y_{\eta 1} \bar{L}_e \tilde{\eta} N_1 + y_{\eta 2} \bar{L}_\mu \tilde{\eta} N_2 + y_{\eta 3} \bar{L}_\tau \tilde{\eta} N_3$$
$$+ y_{12} S N_1 N_2 + y_{13} S^* N_1 N_3 + y_\psi \eta^\dagger \bar{\psi}_{T,R} L_\mu + M_\psi \bar{\psi}_T \psi_T$$
$$+ y_e \bar{L}_e H e_R + y_\mu \bar{L}_\mu H \mu_R + y_\tau \bar{L}_\tau H \tau_R + \text{H.c.}, \quad (1)$$

with $\tilde{\eta} = i\sigma_2 \eta^*$; the scalar potential $V(H, S, \eta)$ is

$$V(H, S, \eta) = -\mu_H^2 (H^\dagger H) + \lambda_1 (H^\dagger H)^2 - \mu_S^2 (S^\dagger S) + \lambda_S (S^\dagger S)^2 + \lambda_{HS} (H^\dagger H)(S^\dagger S)$$
$$+ \mu_\eta^2 (\eta^\dagger \eta) + \lambda_2 (\eta^\dagger \eta)^2 + \lambda_3 (\eta^\dagger \eta)(H^\dagger H)$$
$$+ \lambda_4 (\eta^\dagger H)(H^\dagger \eta) + \frac{\lambda_5}{2} [(H^\dagger \eta)^2 + (\eta^\dagger H)^2] + \lambda_{\eta S} (\eta^\dagger \eta)(S^\dagger S) + \text{H.c.} \quad (2)$$

The SM gauge symmetry is broken by the neutral component of the Higgs doublet H while the Z_4 symmetry is spontaneously broken by the non-zero vacuum expectation value (vev) of the scalar singlet S. Also, we assume $\mu_\eta^2 > 0$ so that η does not acquire any vev. Using Eq. (1), the charged lepton mass matrix M_l, Dirac Yukawa matrix y_D, and right-handed neutrino mass matrix M_R are given by

$$M_l = \frac{1}{\sqrt{2}} \begin{pmatrix} y_e v & 0 & 0 \\ 0 & y_\mu v & 0 \\ 0 & 0 & y_\tau v \end{pmatrix}, \qquad y_D = \begin{pmatrix} y_{\eta 1} & 0 & 0 \\ 0 & y_{\eta 2} & 0 \\ 0 & 0 & y_{\eta 3} \end{pmatrix},$$
$$M_R = \begin{pmatrix} M_{11} & y_{12} v_S/\sqrt{2} & y_{13} v_S/\sqrt{2} \\ y_{12} v_S/\sqrt{2} & 0 & M_{23} e^{i\delta} \\ y_{13} v_S/\sqrt{2} & M_{23} e^{i\delta} & 0 \end{pmatrix}, \quad (3)$$

where $v/\sqrt{2}$ and $v_S/\sqrt{2}$ are vevs of the Higgs field H and scalar field S, respectively, and δ is the phase remaining after redefinition of the fields.

2.1 *Neutrino masses, Muon $(g-2)$, W-boson mass anomaly, and dark matter*

The neutrino masses are generated at the one-loop level (Fig. 1), resulting in the light neutrino mass matrix given by [49,52]

$$M_{ij}^\nu = \sum_k \frac{y_{ik} y_{jk} M_k}{16\pi^2} \left[\frac{M_{\eta_R^0}^2}{M_{\eta_R^0}^2 - M_k^2} \ln \frac{M_{\eta_R^0}^2}{M_k^2} - \frac{M_{\eta_I^0}^2}{M_{\eta_I^0}^2 - M_k^2} \ln \frac{M_{\eta_I^0}^2}{M_k^2} \right], \quad (4)$$

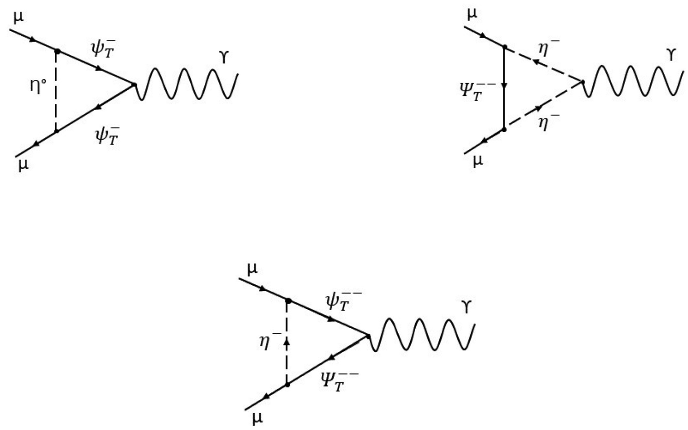

Fig. 2. Diagrams indicating the positive contribution from ψ_T and η to Muon $(g-2)$ at the one-loop level.

where M_k is the mass of kth right-handed neutrino and $M_{\eta_R^0,\eta_I^0}$ are the masses of the real and imaginary parts of the inert doublet η. The Yukawa couplings appearing in Eq. (4) are derived from y_D in the basis where M_R is diagonal. If the mass-squared difference between η_R^0 and η_I^0, i.e., $M^2_{\eta_R^0} - M^2_{\eta_I^0}$, equals $\lambda_5 v^2 << M^2$, where $M^2 = (M^2_{\eta_R^0} + M^2_{\eta_I^0})/2$, then the above expression reduces to

$$M^{\nu}_{ij} = \frac{\lambda_5 v^2}{16\pi^2} \sum_k \frac{y_{ik} y_{jk} M_k}{M^2 - M_k^2} \left[1 - \frac{M_k^2}{M^2 - M_k^2} \ln \frac{M^2}{M_k^2} \right]. \tag{5}$$

The low-energy effective neutrino mass matrix M^{ν} obtained using Eq. (5) can be diagonalized to ascertain model predictions for neutrino masses and mixing angles, namely,

$$M^{\nu} = U M_d^{\nu} U^T, \tag{6}$$

where U is a unitary matrix and $M_d^{\nu} = \mathrm{diag}(m_1, m_2, m_3)$, m_i are neutrino mass eigenvalues. In term of the elements of the diagonalizing matrix,

$$U = \begin{pmatrix} U_{e1} & U_{e2} & U_{e3} \\ U_{\mu 1} & U_{\mu 2} & U_{\mu 3} \\ U_{\tau 1} & U_{\tau 2} & U_{\tau 3} \end{pmatrix}, \tag{7}$$

the neutrino mixing angles can be evaluated using

$$\sin^2\theta_{13} = |U_{e3}|^2, \quad \sin^2\theta_{23} = \frac{|U_{\mu 3}|^2}{1 - |U_{e3}|^2}, \quad \sin^2\theta_{12} = \frac{|U_{e2}|^2}{1 - |U_{e3}|^2}. \tag{8}$$

2.1.1 *Contribution to Muon $(g-2)$.* In order to accommodate Muon $(g-2)$ in the model, we have added a VLL triplet ψ_T with an appropriate Z_4 charge so that it only couples to the muon. This VLL ψ_T alone gives a negative contribution to Muon $(g-2)$ [53]. Also, the charged component of the scalar doublet η has a negative contribution to Muon $(g-2)$. However, ψ_T coupling with η may result in a chirally enhanced positive contribution to Δa_μ through the $y_\psi \eta^\dagger \bar{\psi}_{T,R} L_\mu$ term in Eq. (1). The possible diagrams contributing to Muon $(g-2)$ are shown in Fig. 2.

The contribution to the muon anomalous magnetic moment is given by [53]:

$$\Delta a_\mu = \frac{m_\mu^2 y_\psi^2}{32\pi^2 M_\eta^2} \left[5F_{FFS}\left(M_\psi^2/M_\eta^2\right) - 2F_{SSF}\left(M_\psi^2/M_\eta^2\right) \right], \tag{9}$$

where m_μ, M_ψ, M_η are the masses of the muon, VLL triplet ψ_T, and inert scalar doublet η, respectively, and y_ψ is the coupling constant. Also,

$$F_{FFS}(t) = \frac{1}{6(t-1)^4}[t^3 - 6t^2 + 3t + 2 + 6t \ln t],$$

and

$$F_{SSF}(t) = \frac{1}{6(t-1)^4}[-2t^3 - 3t^2 + 6t - 1 + 6t^2 \ln t], \tag{10}$$

where $t = \frac{M_\psi^2}{M_\eta^2}$ and $M_\eta \approx M_{\eta_R^0}$.

Furthermore, the doubly charged fermion ψ_T^{--} contributing to Muon $(g-2)$ is accessible at collider experiments. In the composite framework of leptons and quarks, the doubly charged fermion ψ_T^{--} couples to SM fermions via the W-boson, leading to single decay channel $\psi_T^{--} \to W^- l^-$, where l is an SM lepton. The production and decay channels of ψ_T^{--} and its antiparticle ψ_T^{++} are given by

$$\bar{u}d \to \psi_T^{--} l^+ \to W^- l^- l^+,$$

$$u\bar{d} \to \psi_T^{++} l^- \to W^+ l^+ l^-,$$

where u (d) are up (down) quarks. In a pp-collider, though the cross-sections for the ψ_T^{--}/ψ_T^{++} decay channels are very small at the parton level, the cross-section corresponding to ψ_T^{++} is relatively large. This particular decay channel contains tri-leptons with same-sign di-leptons having low SM background and a clear signature signal given by $pp \to l^-(l^+l^+)\nu_l$ [54].

2.1.2 *W-boson mass correction from the scalar doublet.* In the scotogenic model, the scalar doublet η provides a correction to the W-boson mass. The NP contribution is parameterized in terms of three self-energy parameters called "oblique parameters", namely, S, T, and U [55]. The correction to the W-boson mass in terms of these parameters is given by [55]

$$M_{\mathrm{W}} = M_{\mathrm{W}}^{\mathrm{SM}} \left[1 - \frac{\alpha_{\mathrm{em}}}{4\left(c_w^2 - s_w^2\right)}(S - 1.55T - 1.24U)\right] \tag{11}$$

where $M_{\mathrm{W}}^{\mathrm{SM}}$ is the mass of the W-boson in the SM, α_{em} is the electromagnetic fine structure constant, and c_w and s_w are the cos and sin of the Weinberg angle, respectively. The values of the oblique parameters, including the new CDF-II W-boson mass result [56], are

$$S = 0.06 \pm 0.10, \quad T = 0.11 \pm 0.12, \quad \text{and} \quad U = 0.14 \pm 0.09, \tag{12}$$

with the correlation coefficients

$$\rho_{ST} = 0.90, \quad \rho_{SU} = -0.59, \quad \text{and} \quad \rho_{TU} = -0.85. \tag{13}$$

With vanishing U, the values of the S and T parameters are found to be [56]

$$S = 0.15 \pm 0.08 \quad \text{and} \quad T = 0.27 \pm 0.06 \quad \text{with correlation coefficient} \quad \rho_{ST} = 0.93. \tag{14}$$

Within the paradigm of the scotogenic model, the main contribution to the oblique parameters comes from the scalar doublet η. The S, T, and U contributions from the scalar doublet η have been derived assuming degenerate CP-even and CP-odd scalars ($M_{\eta_R^0} \simeq M_{\eta_I^0}$), since λ_5 is considered to be small. The S, T, and U corrections are given by [57]

Table 2. The ranges of parameters used in the numerical analysis ($k = 1, 2, 3$, $x \equiv \frac{y_{12} v_S}{\sqrt{2}}$, and $y \equiv \frac{y_{13} v_S}{\sqrt{2}}$).

Parameters	Range
(M_{11}, M_{23})	(10, 100) GeV
(x, y)	(10, 100) GeV
δ°	(0, 360)
$y_{\eta k}$	$(10^{-2}, 10^{-1})$
μ_η	(10, 100) GeV
v_S	(100, 400) GeV
$\lambda_{\eta S}$	$(10^{-2}, 10^{-1})$
λ_3	$(10^{-2}, 10^{-1})$
λ_4	$(10^{-1}, 1)$
λ_5	$(10^{-5}, 5 \times 10^{-5})$
M_k	$(1 \times 10^7, 9 \times 10^7)$ GeV
M_ψ	(100, 400) GeV

$$
\begin{aligned}
S &\simeq \frac{1}{12\pi} \log\left(\frac{M^2}{M_{\eta^+}^2}\right), \\
T &\simeq \frac{2\sqrt{2} G_F}{(4\pi)^2 \alpha_{\text{em}}} \left[\frac{M^2 + M_{\eta^+}^2}{2} - \frac{M^2 M_{\eta^+}^2}{M_{\eta^+}^2 - M^2} \log\left(\frac{M_{\eta^+}^2}{M^2}\right)\right], \\
U &\simeq \frac{1}{12\pi}\left[-\frac{5M_{\eta^+}^4 - 22 M_{\eta^+}^2 M^2 + 5M^4}{3(M_{\eta^+}^2 - M^2)^2} + \frac{(M_{\eta^+}^2 + M^2)(M_{\eta^+}^4 - 4M_{\eta^+}^2 M^2 + M^4)}{(M_{\eta^+}^2 - M^2)^3} \log\left(\frac{M_{\eta^+}^2}{M^2}\right)\right],
\end{aligned} \tag{15}
$$

where $M^2 = (M_{\eta_R^0}^2 + M_{\eta_I^0}^2)/2$ and M_{η^+} is the mass of the charged component of the inert doublet η.

3. Numerical analysis and discussion

In order to constrain the allowed parameter space and investigate the neutrino phenomenology, the model predictions for neutrino mass-squared differences (Δm_{21}^2, Δm_{31}^2) and mixing angles ($\theta_{13}, \theta_{23}, \theta_{12}$) are compared with 3σ ranges of the experimental data on neutrino masses and mixings, namely [58],

$$
\begin{aligned}
&\sin^2\theta_{13} = (0.020\,34 - 0.024\,30), \quad \sin^2\theta_{23} = (0.407 - 0.620), \quad \sin^2\theta_{12} = (0.269 - 0.343), \\
&\Delta m_{31}^2 = (2.431 - 2.599) \times 10^{-3}\,\text{eV}^2, \quad \Delta m_{21}^2 = (6.82 - 8.04) \times 10^{-5}\,\text{eV}^2.
\end{aligned} \tag{16}
$$

The model predictions for neutrino masses and mixing angles are obtained by numerically diagonalizing the low-energy effective neutrino mass matrix in Eq. (5). The free parameters of the model are varied randomly in the ranges given in Table 2. The model predicts neutrino mixing angles and mass-squared differences within their 3σ range. For the sake of completeness, we have given correlation plots depicting the allowed parameter space of the model. Figure 3(a) shows the variation of $\sin^2\theta_{12}$ and $\sin^2\theta_{23}$ with the sum of active neutrino masses Σm_i, whereas Fig. 3(b) shows the variation of $\sin^2\theta_{13}$ with the sum of active neutrino masses Σm_i.

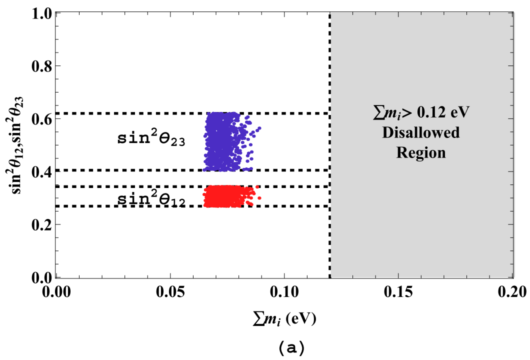

Fig. 3. The correlation of $\sin^2\theta_{12}$, $\sin^2\theta_{23}$, and $\sin^2\theta_{13}$ with the sum of neutrino masses Σm_i. The horizontal lines show the allowed 3σ ranges of the mixing angles [58] and the gray shaded region is disallowed by the cosmological bound on the sum of neutrino masses [59, 60].

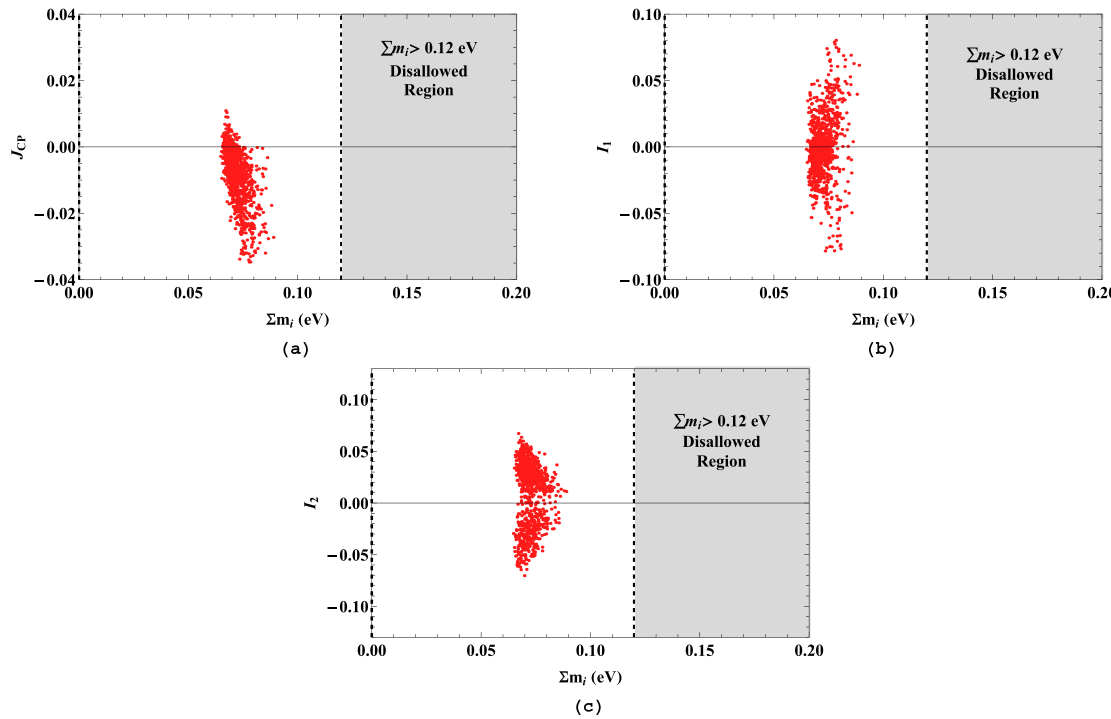

Fig. 4. The correlations of CP-rephasing invariants J_{CP}, I_1, and I_2 with the sum of neutrino masses Σm_i. The gray shaded region is disallowed by the cosmological bound on the sum of neutrino masses [59, 60].

Also, information about the CP violation is encoded in CP-rephasing invariants J_{CP}, I_1, and I_2. The Jarlskog CP invariant J_{CP} is given by [61,62]

$$J_{CP} = \mathrm{Im}\left[U_{e1}U_{\mu 2}U_{e2}^{*}U_{\mu 1}^{*}\right], \tag{17}$$

while the other two CP invariants I_1, I_2 related to Majorana phases can be written as

$$I_1 = \mathrm{Im}\left[U_{e1}^{*}U_{e2}\right], \qquad I_2 = \mathrm{Im}\left[U_{e1}^{*}U_{e3}\right]. \tag{18}$$

Figure 4(a) shows the variation of the Jarlskog CP invariant with the sum of active neutrino masses Σm_i and Figs. 4(b) and (c) show the correlation of I_1 and I_2 with the sum of active neutrino masses Σm_i. The model predicts both CP-conserving and -violating solutions.

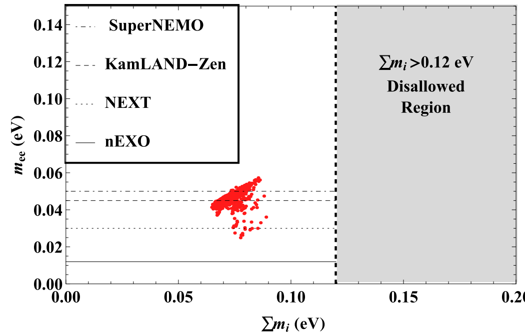

Fig. 5. The correlation of m_{ee} with the sum of neutrino masses Σm_i. The sensitivity reaches of various $0\nu\beta\beta$ decay experiments are shown with the horizontal lines. The gray shaded region is disallowed by the cosmological bound on the sum of neutrino masses [59, 60].

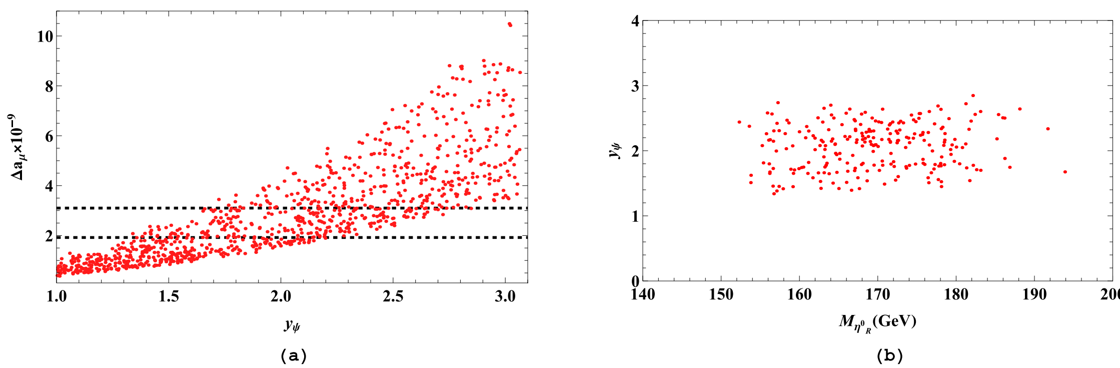

Fig. 6. The variation of the muon anomalous magnetic moment Δa_μ with the coupling constant y_ψ (a). The horizontal lines depict the experimental range of the muon anomalous magnetic moment [1]. The region of the parameter space in the ($M_{\eta_R^0}$–y_ψ) plane is in consonance with Muon $(g-2)$ and neutrino oscillation data (b).

There is also a longstanding question in particle physics about the exact nature of neutrinos. The neutrinoless double beta decay ($0\nu\beta\beta$) experiment can confirm the Majorana nature of the neutrino. The amplitude of this process is proportional to the (1,1) element of the neutrino mass matrix, for which the general expression is given by

$$m_{ee} \equiv M_{11}^{\nu} = \left| \sum_{i=1}^{3} U_{ei}^2 m_i \right| . \tag{19}$$

The correlation of m_{ee} with the sum of active neutrino masses Σm_i is shown in Fig. 5. The sensitivities of $0\nu\beta\beta$ decay experiments such as nEXO [63], NEXT [64, 65], KamLand-Zen [66], and SuperNEMO [67] are also shown in Fig. 5. The model predicts a lower bound $m_{ee} >$ 0.025 eV at 3σ, which is well within the sensitivity reach of the $0\nu\beta\beta$ decay experiments.

3.1 *Muon $(g-2)$*

The contribution to Muon $(g-2)$ is calculated using Eq. (9). In Fig. 6(a), we show the correlation of the muon anomalous magnetic moment Δa_μ with the coupling constant y_ψ. Figure 6(b) depicts the region of the parameter space in the ($M_{\eta_R^0}$–y_ψ) plane, which is consistent with the observed range of Δa_μ. The parameter spaces shown in Figs. 6(a) and (b) have been obtained by requiring the model to be consistent with neutrino oscillation data (16). It is evident from

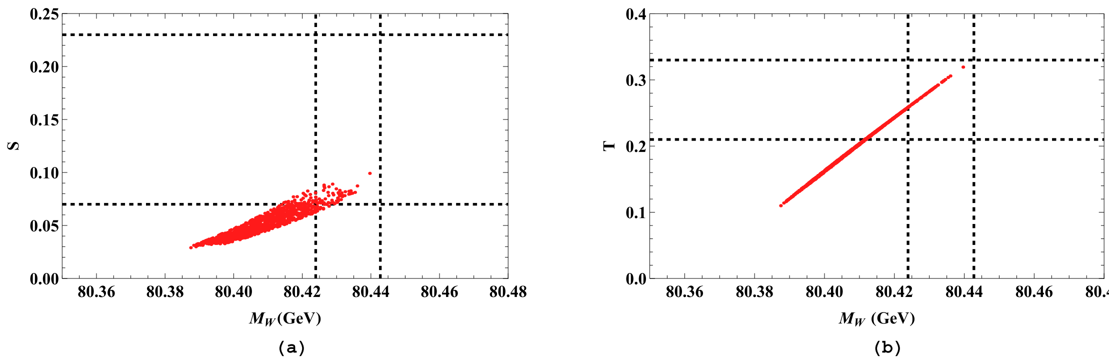

Fig. 7. The correlation of oblique parameters S and T with the W-boson mass M_{W}. The dashed lines indicate the experimental ranges of the oblique parameters (horizontal) [56] and the CDF-II W-boson mass (vertical) [17].

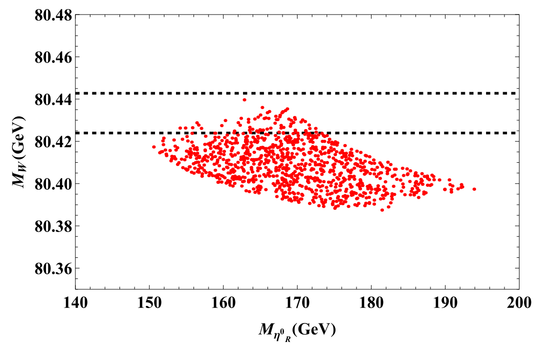

Fig. 8. The correlation of the mass of the real part of the inert doublet $M_{\eta_R^0}$ with the W-boson mass M_{W}. The horizontal dashed lines indicate the CDF-II W-boson mass range [17].

Figs. 6(a) and (b) that the model explains the muon anomalous magnetic moment Δa_μ for 1.3 $< y_\psi <$ 2.8 and a DM candidate mass in the range 152 GeV $< M_{\eta_R^0} <$ 195 GeV, respectively.

3.2 *W-boson mass anomaly*

The corrections to the W-boson mass and oblique parameters reflecting the NP contribution are obtained using Eqs. (11) and (15), respectively. In Figs. 7(a) and (b), we show the correlations of oblique parameters S and T with the W-boson mass M_{W}. The dashed lines depict the experimental ranges of the respective parameters. The parameter space shown in Figs. 7(a) and (b) is also consistent with the Muon $(g-2)$ and neutrino oscillation data. Further, it depicts the region accommodating the CDF-II W-boson mass range and oblique parameters S and T predicted by the model. Figure 8 shows the variation of the W-boson mass M_{W} with the mass of the real part of the inert doublet $M_{\eta_R^0}$ (DM candidate). The dashed lines represent the experimental range of the W-boson mass. It can be seen from Fig. 8 that the explanation of the W-boson mass anomaly further constrains the DM candidate mass, $M_{\eta_R^0}$, to be in the range 154 GeV $< M_{\eta_R^0} <$ 174 GeV, in comparison to the range exhibited in Fig. 6(b) (152 GeV $< M_{\eta_R^0} <$ 195 GeV).

3.3 *Dark matter*

Within the model, the interaction of DM with SM particles may be through two portals, namely, the Higgs portal and the lepton portal via the VLL triplet ψ_T. As discussed ear-

Table 3. The values of input parameters used to obtain a benchmark point for the numerical analysis (k = 1, 2, 3).

Parameters	Value
(M_{11}, M_{23})	(50.9, 68.4) GeV
(x, y)	(63.7, 25.5) GeV
δ°	333.4
$y_{\eta k}$	(0.03, 0.05, 0.05)
$(M_{\eta_R^0}, M_{\eta_I^0})$	(165.93, 165.94) GeV
v_S	116 GeV
M_k	$(8.64, 2.30, 7) \times 10^7$ GeV
M_ψ	269 GeV

lier, the real part of the inert doublet is the lightest among all the BSM fields and is a suitable DM candidate in the model. The mass of DM predicted by the model is in the range 154 GeV $< M_{\eta_R^0} <$ 174 GeV, which is in consonance with neutrino oscillation data and Muon $(g-2)$ and explains the W-boson mass anomaly simultaneously. However, in the context of the inert Higgs doublet model (IHDM), this region (corresponding to the desert region) does not give the correct relic density due to annihilation of the DM particle into gauge bosons [68, 69]. This issue can be resolved by considering a different production mechanism of DM [70, 71] or by extending the IHDM with multi-component bosonic DM, which provides the required relic density in the desert region [72]. Assuming non-thermal production of DM, the relic density is approximately given by [70]

$$\Omega h^2 = \frac{M_{\rm DM} Y_0 s_0}{\rho_c}, \tag{20}$$

where $M_{\rm DM} = M_{\eta_R^0}$ is the mass of DM, Y_0 is the co-moving number density or yield of DM, $s_0 \sim 2891.2\text{cm}^{-3}$ is the present-day entropy of the universe, $\rho_c \sim 1.05 \times 10^{-5} h^2$ GeV cm^{-3} is the critical density, and $h \sim 0.72$ is the Hubble parameter. The predicted mass of DM along with Eq. (20) can be used to get a crude approximation for the relic density of DM. For example, the present model accommodates an observed relic density of DM $\sim \mathcal{O}(0.12)$ for $Y_0 \sim \mathcal{O}(10^{-12})$, which can be achieved through non-thermal production mechanisms [71]. It is interesting to note, from the above order-of-magnitude analysis, that the model can explain the relic density of DM in the desert region, thus warranting further detailed study in future work.

Benchmark point: For ready reference, we provide a benchmark point for which the model satisfies the neutrino oscillation data, Muon $(g-2)$, and the W-boson mass anomaly, simultaneously. For the input parameters listed in Table 3, the neutrino mixing angles and mass-squared differences predicted by the model are

$$\sin^2\theta_{13} = 0.022, \quad \sin^2\theta_{23} = 0.60, \quad \sin^2\theta_{12} = 0.34,$$

$$\Delta m_{31}^2 = 2.46 \times 10^{-3}\,\text{eV}^2, \quad \Delta m_{21}^2 = 7.1 \times 10^{-5}\,\text{eV}^2.$$

The value of $\Delta a_\mu = 2.96 \times 10^{-9}$ for $M_\psi = 269$ GeV, $M_\eta = 101$ GeV, and $y_\psi = 2.57$ while the mass of the W-boson $M_{\rm W} = 80.43$ GeV for the oblique parameters $S = 0.08$ and $T = 0.29$.

Finally, a comment on the lepton flavor violation (LFV) process $\mu \to e\gamma$ is in order. The investigation of the lepton flavor violation (LFV) process is encouraging from the perspective of explorable signatures of BSM scenarios at collider experiments. Any detection of such LFV decays as $\mu \to e\gamma$ will be a new physics signature. Within the model proposed in this work, the charged component of the scalar doublet can provide such an NP contribution, for which the decay width is given by [73, 74]

$$\mathrm{Br}(\mu \to e\gamma) = \frac{3(4\pi)^3 \alpha_{\mathrm{em}}}{4G_F^2} |A_D|^2 \mathrm{Br}(\mu \to e\nu_\mu \bar{\nu_e}), \tag{21}$$

where

$$A_D = \sum_k \frac{y_{ke}^* y_{k\mu}}{16\pi^2} \frac{1}{M_{\eta^+}^2} f(x'), \tag{22}$$

G_F is the Fermi constant, $x' = M_k^2/M_{\eta^+}^2$, and $f(x') = \frac{1-6x'+3x'^2+2x'^3-6x'^2\log x'}{12(1-x')^4}$. The LFV prediction of the model is found to be in consonance with the experimental bound (in fact less than 10^{-14}) for the obtained DM mass range.

4. Conclusions

The muon $(g-2)$ anomaly, neutrino mass and mixing pattern, and dark matter lack an explanation within the SM. Also, recent observation of the W-boson anomaly requires new physics explanation beyond the SM. In this work, we propose a scotogenic scenario explaining neutrino oscillation data, the Muon $(g-2)$ result, and the W-boson mass anomaly with a possible DM candidate simultaneously. The SM gauge group is extended with Z_4 symmetry, which is broken by the vev of the scalar singlet S. In particular, to accommodate small neutrino masses and DM in the model, we have considered a scotogenic model that includes three right-handed neutrinos and an inert scalar doublet that is odd under Z_2 symmetry. The real part of the inert doublet is the lightest Z_2-odd particle; thus, it is a suitable DM candidate in the model. Furthermore, a VLL triplet ψ_T is introduced that couples to the scalar doublet, providing a positive contribution to Muon $(g-2)$. We also provide a benchmark point for the numerical analysis, indicating the simultaneous explanation of the above-mentioned anomalies. In addition, the implications of the model for $0\nu\beta\beta$ decay have been studied. The model predicts a lower bound $m_{ee} > 0.025$ eV at 3σ, which is well within the sensitivity reach of the $0\nu\beta\beta$ decay experiments. The model, in general, predicts both CP-conserving and CP-violating solutions. The model explains the muon anomalous magnetic moment Δa_μ for $1.3 < y_\psi < 2.8$ and a DM candidate mass in the range 152 GeV $< M_{\eta_R^0} <$ 195 GeV (Fig. 6(b)). The explanation of the W-boson mass anomaly further constrains the mass of the DM candidate, $M_{\eta_R^0}$, to be in the range 154 GeV $< M_{\eta_R^0} <$ 174 GeV (Fig. 8).

Acknowledgements

S.A. acknowledges the financial support provided by the Central University of Himachal Pradesh. M.K. acknowledges the financial support provided by the Department of Science and Technology, Government of India under Grant No. DST/INSPIRE Fellowship/2018/IF180327. The authors also acknowledge the Department of Physics and Astronomical Science for providing the necessary facilities to carry out this work. B.C.C. is also grateful to the Inter University Centre for Astronomy and Astrophysics (IUCAA) for providing necessary facilities during the completion of this work.

Funding

Open Access funding: SCOAP^3.

References

1 B. Abi et al. [Muon $g-2$ Collaboration], Phys. Rev. Lett. **126**, 141801 (2021).
2 T. Aoyama et al., Phys. Rept. **887**, 1 (2020).
3 T. Abe, R. Sato, and K. Yagyu, J. High Energy Phys. **1707**, 012 (2017).
4 P. T. P. Hutauruk, D. W. Kang, J. Kim, and H. Okada, arXiv:2012.11156 [hep-ph] [Search inSPIRE].
5 L. Calibbi, M. L. López-Ibáñez, A. Melis, and O. Vives, Eur. Phys. J. C **81**, 929 (2021).
6 B. D. Sáez and K. Ghorbani, Phys. Lett. B **823**, 136750 (2021).
7 X. G. He, G. C. Joshi, H. Lew, and R. R. Volkas, Phys. Rev. D **43**, 22 (1991).
8 X. G. He, G. C. Joshi, H. Lew, and R. R. Volkas, Phys. Rev. D **44**, 2118 (1991).
9 D. Borah, A. Dasgupta, and D. Mahanta, Phys. Rev. D **104**, 075006 (2021).
10 A. Biswas, S. Choubey, and S. Khan, J. High Energy Phys. **1609**, 147 (2016).
11 S. Zhou, Chin. Phys. C **46**, 011001 (2022).
12 W. L. Guo, Z. z. Xing, and S. Zhou, Int. J. Mod. Phys. E **16**, 1 (2007).
13 A. Dev, arXiv:1710.02878 [hep-ph] [Search inSPIRE].
14 C. Majumdar, S. Patra, P. Pritimita, S. Senapati, and U. A. Yajnik, J. High Energy Phys. **2009**, 010 (2020).
15 S. Patra, S. Rao, N. Sahoo, and N. Sahu, Nucl. Phys. B **917**, 317 (2017).
16 P. A. Zyla et al. [Particle Data Group], Prog. Theor. Exp. Phys. **2020**, 083C01 (2020).
17 T. Aaltonen et al. [CDF Collaboration], Science **376**, 170 (2022).
18 S. Centelles Chuliá, R. Srivastava, and S. Yadav, arXiv:2206.11903 [hep-ph] [Search inSPIRE].
19 S. Yaser Ayazi and M. Hosseini, arXiv:2206.11041 [hep-ph] [Search inSPIRE].
20 S. S. Afonin, arXiv:2205.12237 [hep-ph] [Search inSPIRE].
21 J. Kawamura and S. Raby, arXiv:2205.10480 [hep-ph] [Search inSPIRE].
22 J. W. Wang, X. J. Bi, P. F. Yin, and Z. H. Yu, arXiv:2205.00783 [hep-ph] [Search inSPIRE].
23 A. Batra, K. A. ShivaSankar, S. Mandal, H. Prajapati, and R. Srivastava, arXiv:2204.11945 [hep-ph] [Search inSPIRE].
24 D. Borah, S. Mahapatra, and N. Sahu, Phys. Lett. B **831**, 137196 (2022).
25 K. Ghorbani and P. Ghorbani, arXiv:2204.09001 [hep-ph] [Search inSPIRE].
26 D. Borah, S. Mahapatra, D. Nanda, and N. Sahu, arXiv:2204.08266 [hep-ph] [Search inSPIRE].
27 O. Popov and R. Srivastava, arXiv:2204.08568 [hep-ph] [Search inSPIRE].
28 P. Athron, M. Bach, D. H. J. Jacob, W. Kotlarski, D. Stöckinger, and A. Voigt, arXiv:2204.05285 [hep-ph] [Search inSPIRE].
29 N. Chakrabarty, arXiv:2206.11771 [hep-ph] [Search inSPIRE].
30 T. A. Chowdhury and S. Saad, arXiv:2205.03917 [hep-ph] [Search inSPIRE].
31 S. P. He, arXiv:2205.02088 [hep-ph] [Search inSPIRE].
32 R. Dcruz and A. Thapa, arXiv:2205.02217 [hep-ph] [Search inSPIRE].
33 J. Kim, Phys. Lett. B **832**, 137220 (2022).
34 J. Kim, S. Lee, P. Sanyal, and J. Song, arXiv:2205.01701 [hep-ph] [Search inSPIRE].
35 F. J. Botella, F. Cornet-Gomez, C. Miró, and M. Nebot, arXiv:2205.01115 [hep-ph] [Search inSPIRE].
36 Q. Zhou and X. F. Han, arXiv:2204.13027 [hep-ph] [Search inSPIRE].
37 S. Baek, arXiv:2204.09585 [hep-ph] [Search inSPIRE].
38 A. Bhaskar, A. A. Madathil, T. Mandal, and S. Mitra, arXiv:2204.09031 [hep-ph] [Search inSPIRE].
39 X. F. Han, F. Wang, L. Wang, J. M. Yang, and Y. Zhang, arXiv:2204.06505 [hep-ph] [Search inSPIRE].
40 P. Athron, A. Fowlie, C. T. Lu, L. Wu, Y. Wu, and B. Zhu, arXiv:2204.03996 [hep-ph] [Search inSPIRE].
41 J. Cao, L. Meng, L. Shang, S. Wang, and B. Yang, arXiv:2204.09477 [hep-ph] [Search inSPIRE].
42 K. S. Babu, S. Jana, and P. K. Vishnu, arXiv:2204.05303 [hep-ph] [Search inSPIRE].
43 O. Atkinson, M. Black, C. Englert, A. Lenz, and A. Rusov, arXiv:2207.02789 [hep-ph] [Search inSPIRE].
44 D. Borah, M. Dutta, S. Mahapatra, and N. Sahu, Phys. Rev. D **105**, 015029 (2022).
45 S. Jana, P. K. Vishnu, W. Rodejohann, and S. Saad, Phys. Rev. D **102**, 075003 (2020).
46 S. Baek, Phys. Lett. B **756**, 1 (2016).
47 Z. L. Han, R. Ding, S. J. Lin, and B. Zhu, Eur. Phys. J. C **79**, 1007 (2019)

48 D. W. Kang, J. Kim, and H. Okada, Phys. Lett. B **822**, 136666 (2021)
49 E. Ma, Phys. Rev. D **73**, 077301 (2006).
50 G. Cacciapaglia and M. Rosenlyst, J. High Energy Phys. **2109**, 167 (2021).
51 M. Rosenlyst, Phys. Rev. D **106**, 013002 (2022).
52 A. Merle and M. Platscher, J. High Energy Phys. **1511**, 148 (2015).
53 A. Freitas, J. Lykken, S. Kell, and S. Westhoff, J. High Energy Phys. **1405**, 145 (2014); **1409**, 155 (2014) [erratum].
54 S. Biondini, O. Panella, G. Pancheri, Y. N. Srivastava, and L. Fano, Phys. Rev. D **85**, 095018 (2012).
55 M. E. Peskin and T. Takeuchi, Phys. Rev. D **46**, 381 (1992).
56 C. T. Lu, L. Wu, Y. Wu, and B. Zhu, arXiv:2204.03796 [hep-ph] [Search inSPIRE].
57 H. H. Zhang, W. B. Yan, and X. S. Li, Mod. Phys. Lett. A **23**, 637 (2008).
58 I. Esteban, M. C. Gonzalez-Garcia, M. Maltoni, T. Schwetz, and A. Zhou, J. High Energy Phys. **2009**, 178 (2020).
59 E. Giusarma, M. Gerbino, O. Mena, S. Vagnozzi, S. Ho, and K. Freese, Phys. Rev. D **94**, 083522 (2016).
60 N. Aghanim et al. [Planck Collaboration], Astron. Astrophys. **641**, A6 (2020); **652**, C4 (2021) [erratum].
61 P. I. Krastev and S. T. Petcov, Phys. Lett. B **205**, 84 (1988).
62 C. Jarlskog, Phys. Rev. Lett. **55**, 1039 (1985).
63 C. Licciardi [nEXO Collaboration], J. Phys. Conf. Ser. **888**, 012237 (2017).
64 F. Granena et al. [NEXT Collaboration], arXiv:0907.4054 [hep-ex] [Search inSPIRE].
65 J. J. Gomez-Cadenas et al. [NEXT Collaboration], Adv. High Energy Phys. **2014**, 907067 (2014).
66 A. Gando et al. [KamLAND-Zen Collaboration], Phys. Rev. Lett. **117**, 082503 (2016).
67 A. S. Barabash, J. Phys. Conf. Ser. **375**, 042012 (2012).
68 D. Borah and A. Gupta, Phys. Rev. D **96**, 115012 (2017).
69 M. A. Díaz, B. Koch, and S. Urrutia-Quiroga, Adv. High Energy Phys. **2016**, 8278375 (2016).
70 L. Sarma, P. Das, and M. K. Das, Nucl. Phys. B **963**, 115300 (2021).
71 M. Drees, H. Iminniyaz, and M. Kakizaki, Phys. Rev. D **73**, 123502 (2006).
72 S. Chakraborti, A. Dutta Banik, and R. Islam, Eur. Phys. J. C **79**, 662 (2019).
73 T. Toma and A. Vicente, J. High Energy Phys. **1401**, 160 (2014).
74 L. Lavoura, Eur. Phys. J. C **29**, 191 (2003).